TECHNOLOGIES OF HIGH VOLTAGE NEUTRAL BEAM INJECTORS FOR MAGNETIC FUSION DEVICES

O. Sotnikov, A. Sanin, A. Belavsky, Yu. Belchenko, A. Gorbovsky, A. Gmyrya, I. Emelev, R. Finashin, A. Kondakov, I. Shikhovtsev,

V. Amirov, D. Gavrisenko, P. Deichuli, N. Ilyenko

Budker Institute of Nuclear Physics SB RAS

O.Z.Sotnikov@inp.nsk.su

ABSTRACT

INTRODUCTION

and gas from entering the accelerator;

an increased voltage holding are used

The high-energy neutral injectors based on the acceleration of negative ions (N-NBI) are being developed at the Budker Institute of Nuclear Physics (BINP). The special features of the BINP injector are the RF surface-plasma negative ion source with thermostabilisation of electrodes, the low energy beam transport (LEBT) section between the ion source and accelerator and a wide-aperture multielectrode accelerator, pumped from the both sides. The tank of LEBT section is pumped by cryopumps and it diminishes the entering of gas and impurities to accelerator, while dipole magnets installed in LEBT provide the beam turn to the accelerator entrance. It favors the electrical strength of accelerator and the reliability of the source and injector operation. The accelerated negative ion beam is focused by quadrupole lenses and neutralized by a plasma neutralizer, which provides up to 84% neutralization efficiency for energy negative ions >500 keV. The injector line with 9 A negative ion hydrogen beam production and acceleration to 500 keV for 20 s pulse is planned for TRT tokamak. The results of negative ion beam production in the 1.5 A source prototype, 1 A beam transport and acceleration to 400 keV at the BINP accelerator teststand as well as the first experiments on a full-scale 9 A negative ion source are presented.

The powerful negative ion (NI) based injector for plasma heating in

thermonuclear fusion class devices is being developed at the Budker

institute of nuclear physics. The injector implements several original

LEBT section, which purifies the beam and prevents the stray particles

• a wide - aperture multielectrode accelerator with improved pumping and

The study of ion beam production, transport and acceleration is carried out

approaches in general acceleration scheme and ion source design:

on the injector teststand with principal scheme shown in Figure 1.

• the negative ion source is separated from the acceleration tube with

The three-electrodes ion-optical system (IOS) was used to extract and accelerate negative ions from the source. IOS geometry was optimized by the IBSimu code. The IOS extraction gap geometry for one of 21 beamlets of the improved source version is shown in Fig.3. It provides the extraction of the beam with emission current density up to 450 A/m² and the interception of the most of co-extracted electrons. The extraction electrode concavity with radius of 1.75 m provides the beam ballistic focusing. The voltages of extraction gap up to 14 kV and of acceleration gap up to 110 kV were applied.

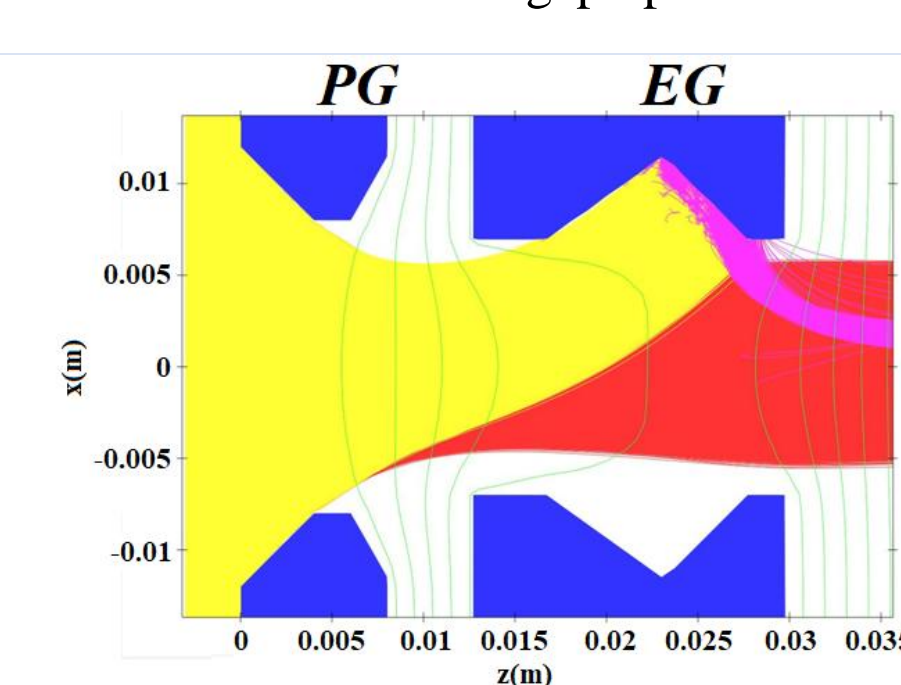


FIG. 3. Beam formation in source extraction gap with the improved geometry. EG voltage 14 kV, EG aperture diameter 14 mm, EG thickness 17 mm. Emission aperture internal diameter 16 mm. H- current density 450 A/cm2. Red lines - H- ions, yellow lines - co-extracted electrons, Magenta *lines – trajectories of secondary emitted electrons*

The improved prototype source routinely produces the H⁻ beams with a current of 1.2 – 1.5 A and the energy up to 120 keV in pulses up to 20 s, as it is illustrated in the oscillogram of Figure 4. The 1.5 A, beam production in long pulse 6.5 sec is shown in Figure 4. Track I_b shows the production of 1.5 A 117 keV H⁻ beam in pulse interval 1 -7.5s with the co- extracted electron current value of $I_e = I_{ex} - I_b \sim 1$ A. About 20% growth of co-extracted electron current from 0.9 to 1.1 A was recorded to the pulse end. The growth is probably caused by PG cesium coverage depletion and it could be compensated by addition of cesium seed. It should be noted that the obtained value of the 1.5 A H⁻ beam at the source exit corresponds to a initial average emission current density of 450 A/m² (taking into account 20% stripping of negative ions on the accompanying gas in the IOS).

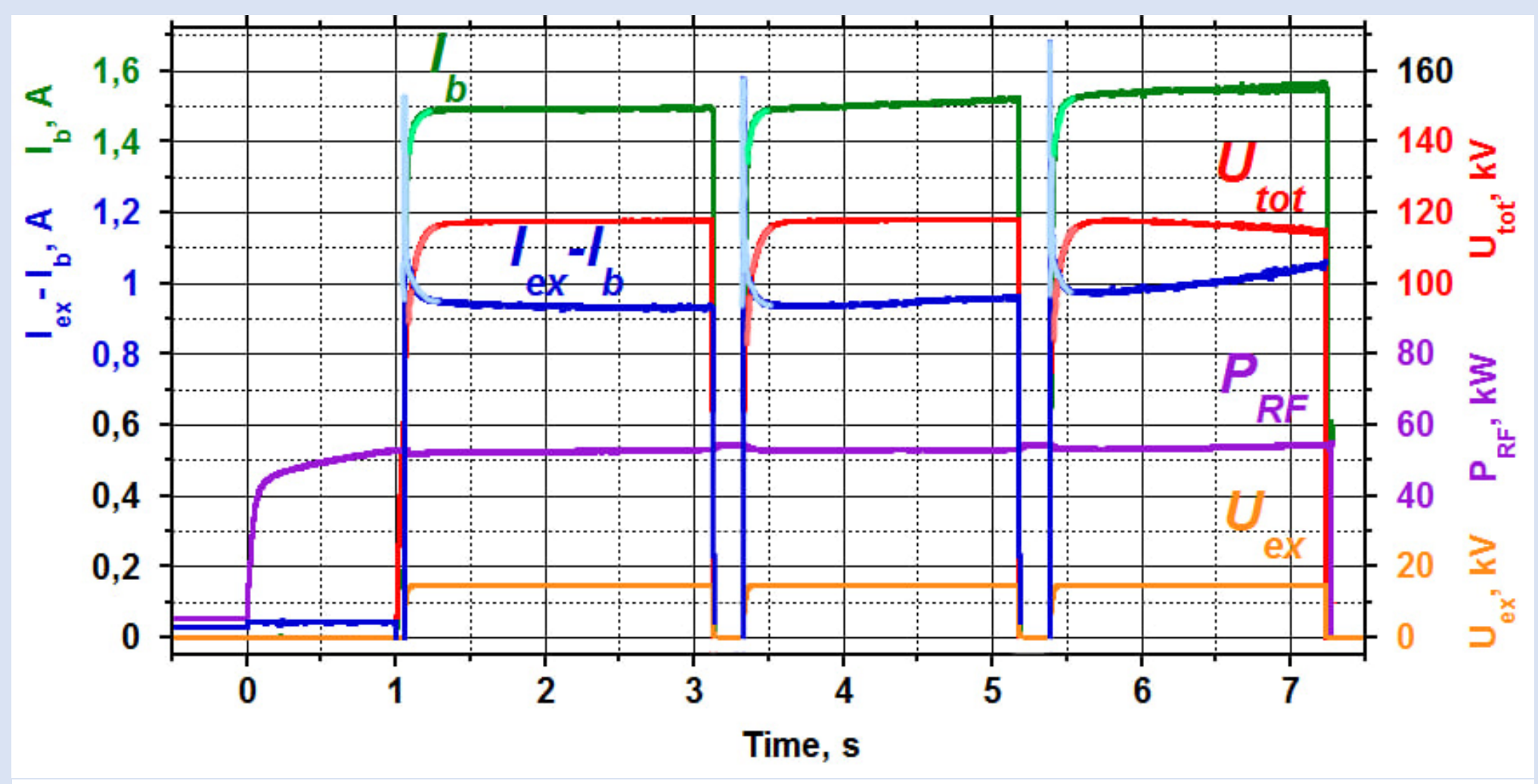


FIG. 4. Oscillogram of the 6 s source pulse with H- beam current of 1.5 A, energy 117 keV.

FIG. 1. Scheme of BINP negative ion based neutral beam injector prototype. The injector teststand equipped with 1.5A prototype ion source and beam line providing up to 1A beam transport and acceleration. The 120 keV 1.5 A negative ion prototype potential. The source is attached to the vacuum tank of LEBT section, which is attached to

10 m

source with it power supplies is located on the high voltage platform, biased up to -400 kV the accelerating tube. LEBT tank is equipped with two bending magnets and high speed pumping system. The accelerating tube was designed to accelerate up to 1 A beam and consists of 9 electrodes with entrance aperture of 200 - 260 mm. The accelerated beam is focused by quadrupoles and passes to calorimeter.

1.5 A NEGATIVE ION SOURCE

The scheme of the negative ion source is shown in Figure 2. The plasma produced by the RF driver flows through an expansion chamber towards the negative ion converter – to the plasma grid, which is covered by cesium layer to enhance negative ion production. The dipole magnetic filter is used to suppress the electron diffusion and to decrease the electron temperature and density in the region of negative ion production near the plasma grid (PG). Cesium is supplied by heating the external ovens with cesium pellets. Cesium vapour feeds through the heated distribution galleries located at the plasma grid periphery. In order to support the PG optimal cesium coverage and to prevent the cesium accumulation on the extraction grid (EG) both PG and EG were kept hot by circulation of hot thermal liquid through the channels drilled in the electrode bodies.

The positive biasing of plasma grid with respect to the expansion chamber is applied in order to collect the plasma electrons and to reduce the flow of electrons co-extracted together with negative ions. The multiaperture extraction of H- ion in the prototype source is provided with the 21 emission apertures having the internal diameter of 16 mm and conical chamfers arranged in a rectangular array on the plasma grid surface

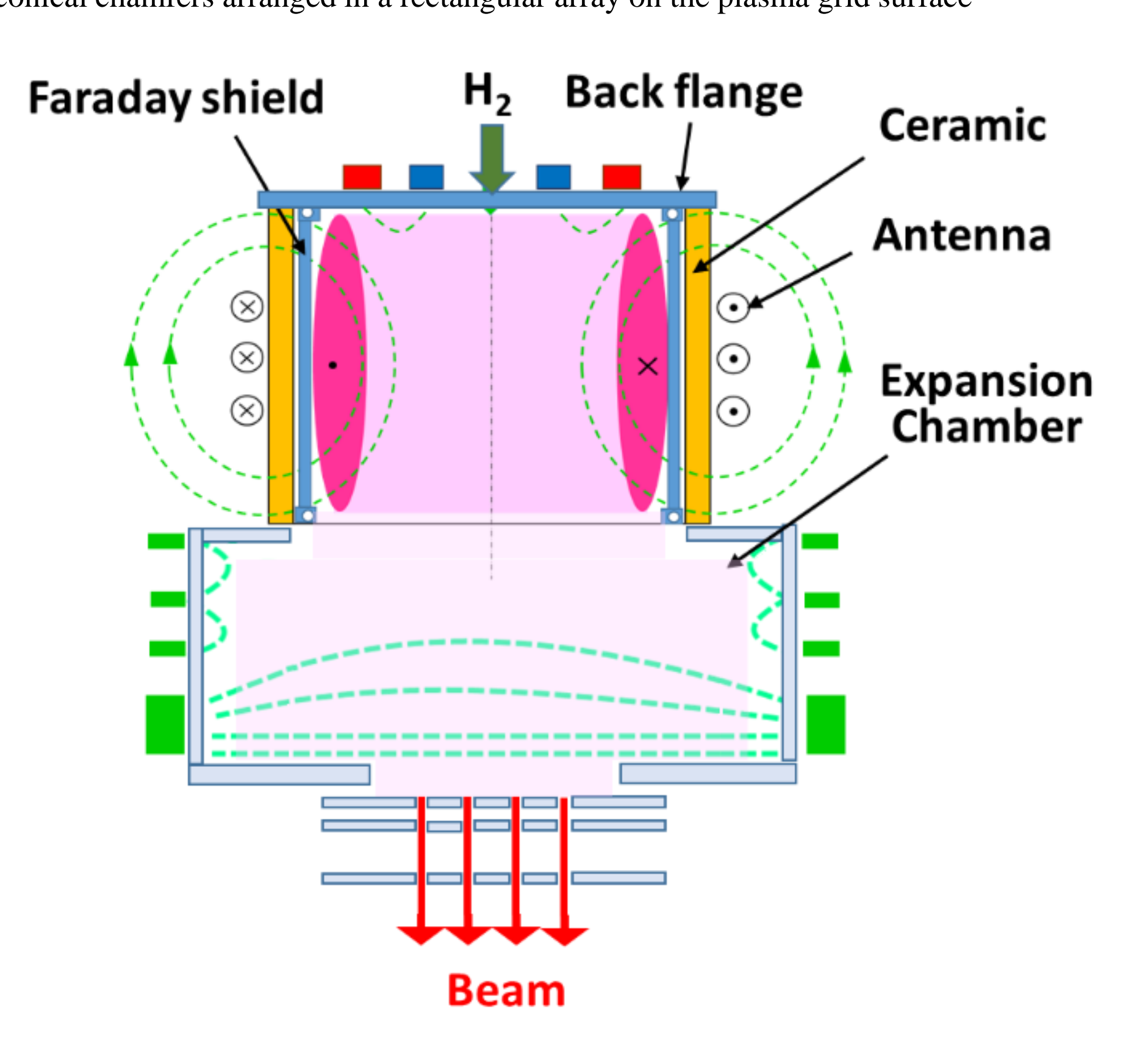


FIG. 2. Scheme of RF negative ion source. Dashed lines -magnetic field of RF antennas and magnetic

The components of inductive 60 kW, 4 MHz RF driver are: 200 mm ceramic tube, a protective Faraday Shield installed inside the ceramic tube to defend it from erosion by plasma. The 3.5 turn water-cooled antenna made of a copper tube with outer diameter of 6 mm and covered by dielectric sleeve. Back flange is shielded by 2 mm molybdenum disc from the plasma side. Hydrogen is puffed into the discharge chamber with the help of electromagnetic valves, attached to the ignition unit. The RF discharge is initiated by spark plasma from the ignition unit. The RF generator delivers output voltage and power up to 14 kV and 75 kW correspondingly. The RF driver elements and material was optimized to enlarge the driver efficiency.

The acceleration grid geometry was changed in order to decrease beam divergence as well. The accelerating electrode with five 16x124 mm slits elongated across magnetic field was changed to 5x5 array of round apertures with diameter 16.5 mm. It decreases the beam divergence, but reduces the gas pumping from the IOS and increases beam stripping. Nevertheless this scheme have provided an effective beam generation with an emission density of 300 A/m² with lower beam divergence.

Figure 5 shows the profiles of the beam, obtained from the source with round apertures (red) and with the slits (blue) in the accelerator grid and transported through the LEBT at the distance 4 m from the source (modelling by IBSimu, initial beam current 1.9 A, emission current density 450 A/m².). In the case of round apertures (red profile in Figure. 5), almost all beam could be transported to the accelerator input with aperture diaphragm ø200mm.

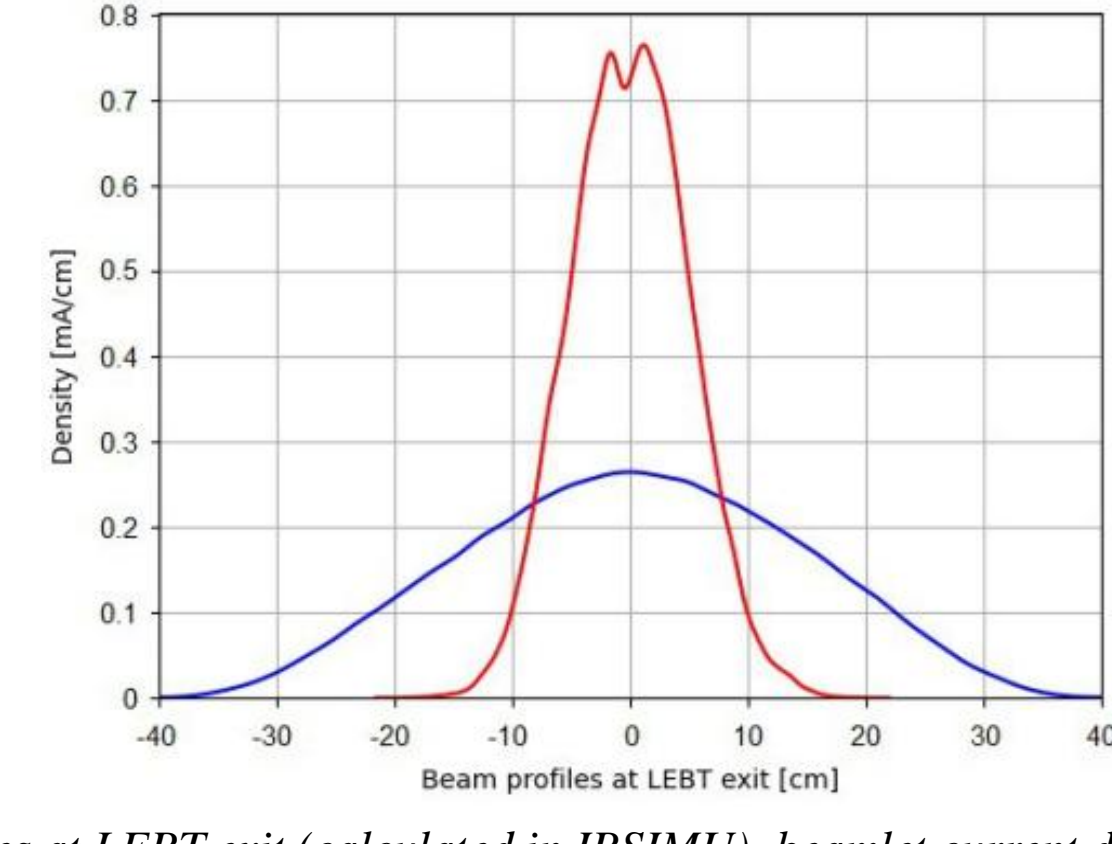


FIG. 5. Beam profiles at LEBT exit (calculated in IBSIMU), beamlet current density 45 mA/cm2. Blue -Acceleration electrode geometry with 5 slits 16 x 124 mm; Red - with 21 apertures with ø16.5 mm.

The parameters of the beam transported through the LEBT was directly measured by movable Faraday Cup (FC), installed in the LEBT at the distance 2.5 m from the source, and by the secondary emission probes, installed around the LEBT exit aperture. Figure 6 shows the 2-dimensional profile of the 1A, 102 kV beam with the lowest divergence, measured by FC for the beam, produced by the source with the round apertures of accelerated grid and by concaved extraction grid. As it is seen from Fig.6, the diameter of the beam in the improved source is about 96 mm (FWHM). The lowest beam divergence of ~15 mrad (Fig.6) was recorded at the optimal extraction voltage of 10 kV. The total current, measured by FC with inlet window ø 170 mm corresponded well with the values, obtained by integration of beam profiles, measured by beam scan with the small collectors installed behind the openings in main FC plate.

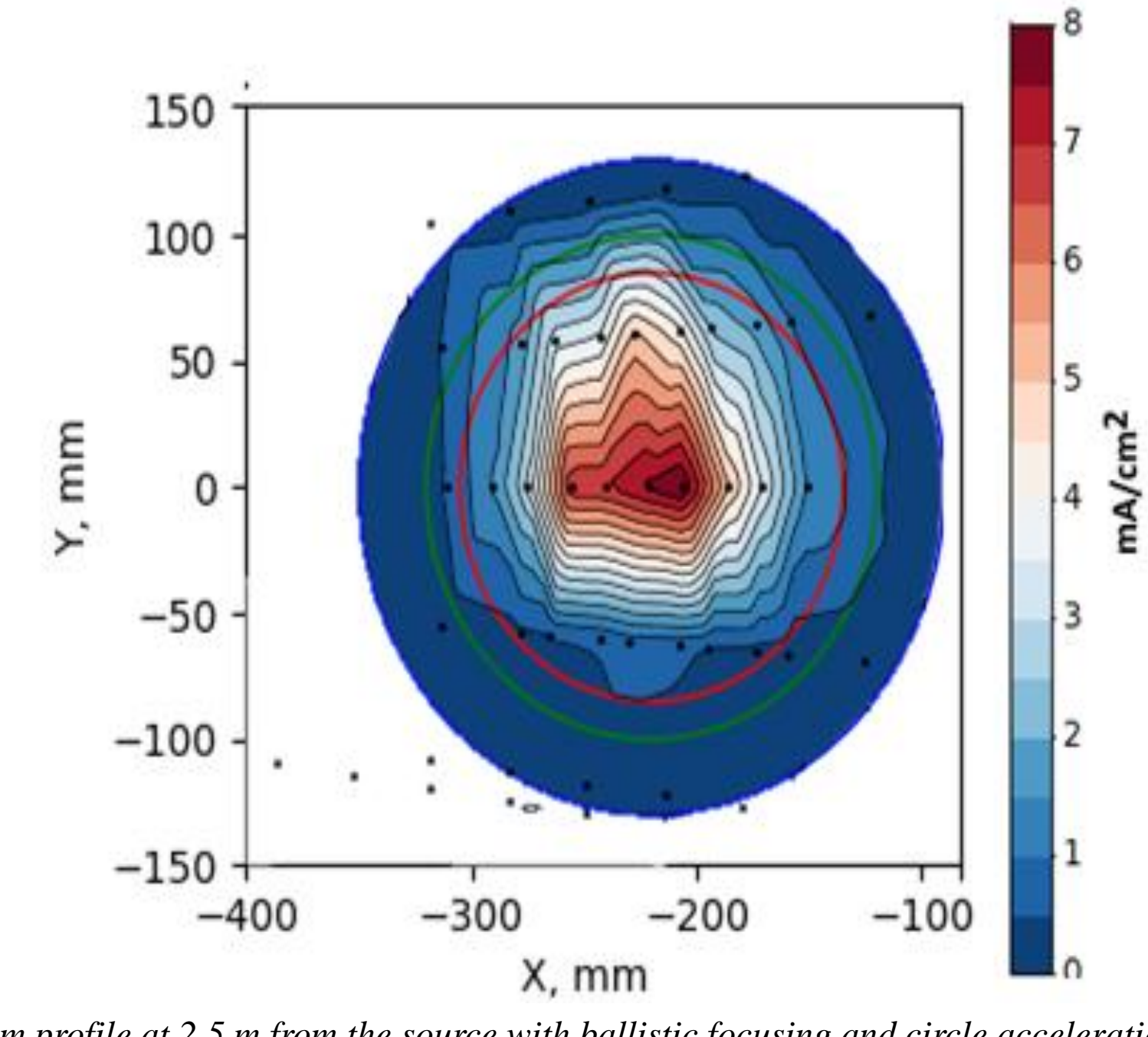


FIG. 6. Beam profile at 2.5 m from the source with ballistic focusing and circle acceleration grid apertures. Probe positions are shown by black dotes. $I_b = 1A$, $U_b = 120 \text{keV}$, $I_{FC} \emptyset 170 = 0.77A$, $U_{ex} = 10 \text{keV}$

The only cryopump with pumping rate of 10⁵ L/sec for hydrogen was used in the case of Fig.6. It provides the residual pressure in the LEBT tank of about $1 \cdot 10^{-3}$ Pa, so $\sim 83\%$ of the beam, outgoing the source was transported to the FC at distance of 2.5 m, and ~ 70% to the accelerator input at distance 4.5 m.

SINGLE APERTURE ACCELERATOR

The H- beam acceleration was performed with the wide single aperture acceleration tube. The cross section of accelerator tube and scheme of electrodes connection to power supply are shown in Figure 7. The currents measured in the circuit of the first accelerator electrode (I_P in Figure 7) and in the circuit of the last accelerating gaps (I_{HV} in Fig.7) were used to evaluate the beam transmission during acceleration. I_p corresponds to the beam current accelerated in the first gap of accelerator, i.e. the current, entering the accelerator, while I_{HV} is the current at the accelerator output, i.e. the final accelerated beam current. The differential current I_{HV} - I_p characterizes the beam losses during acceleration.

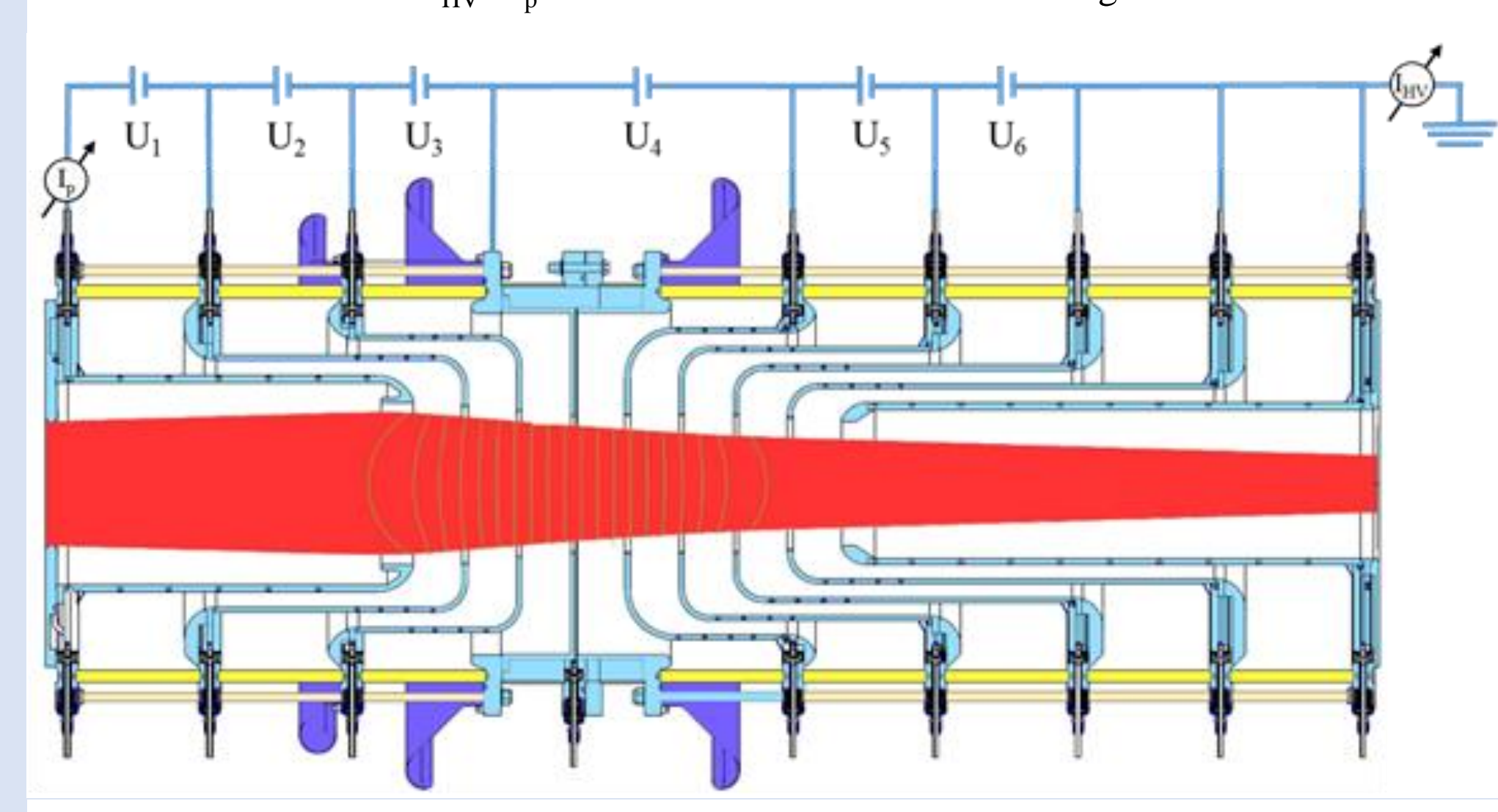


FIG. 7. The acceleration tube cross section with the scheme of electrodes powering and currents measurement. Red and green lines – beam trajectories and electric equipotential of IBSIMU modelling for the beam with the initial divergence 15 mrad with 21 beamlet.

Typical oscillograms of beams outgoing the source I_b , entering the accelerator tube I_p , and outgoing the accelerator I_{HV} are shown in Figure 8. The line U_{HV} shows the accelerator voltage applied. Fig.8 illustrates ~ 76% transport of the 1 A negative ion beam outgoing the source to the accelerator, and acceleration of $0.65 \div 0.75$ A beam to total energy of ~400 keV. The recorded 76% beam pass through the LEBT is in a good agreement with ~ 24% stripping on LEBT residual gas.

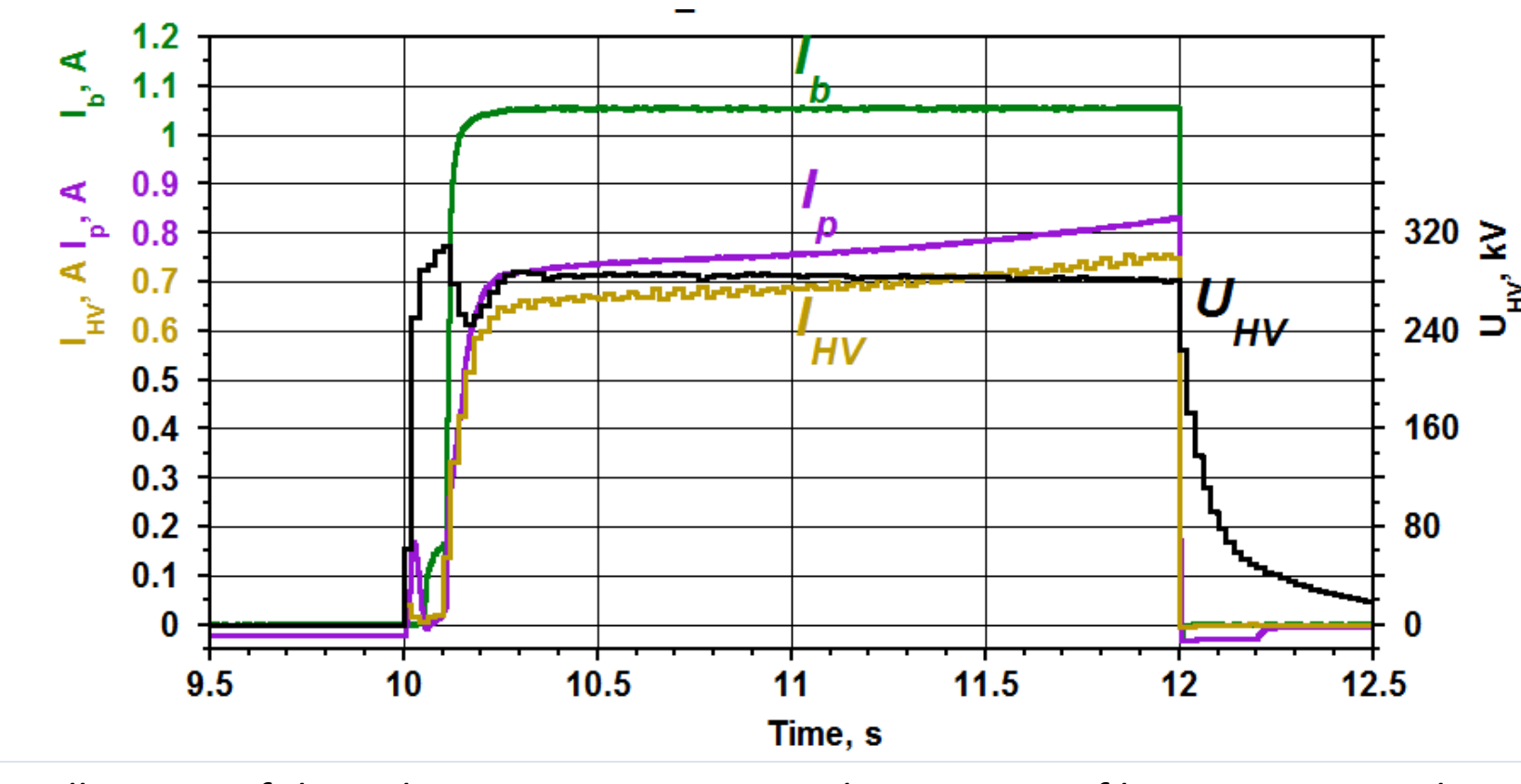


FIG. 8. Oscillograms of the NI beam current outgoing the source I_b of beam current at the input of the accelerator I_n and of beam current I_{HV} accelerated to energy 0.4 MeV. U_{HV} – acceleration voltage.

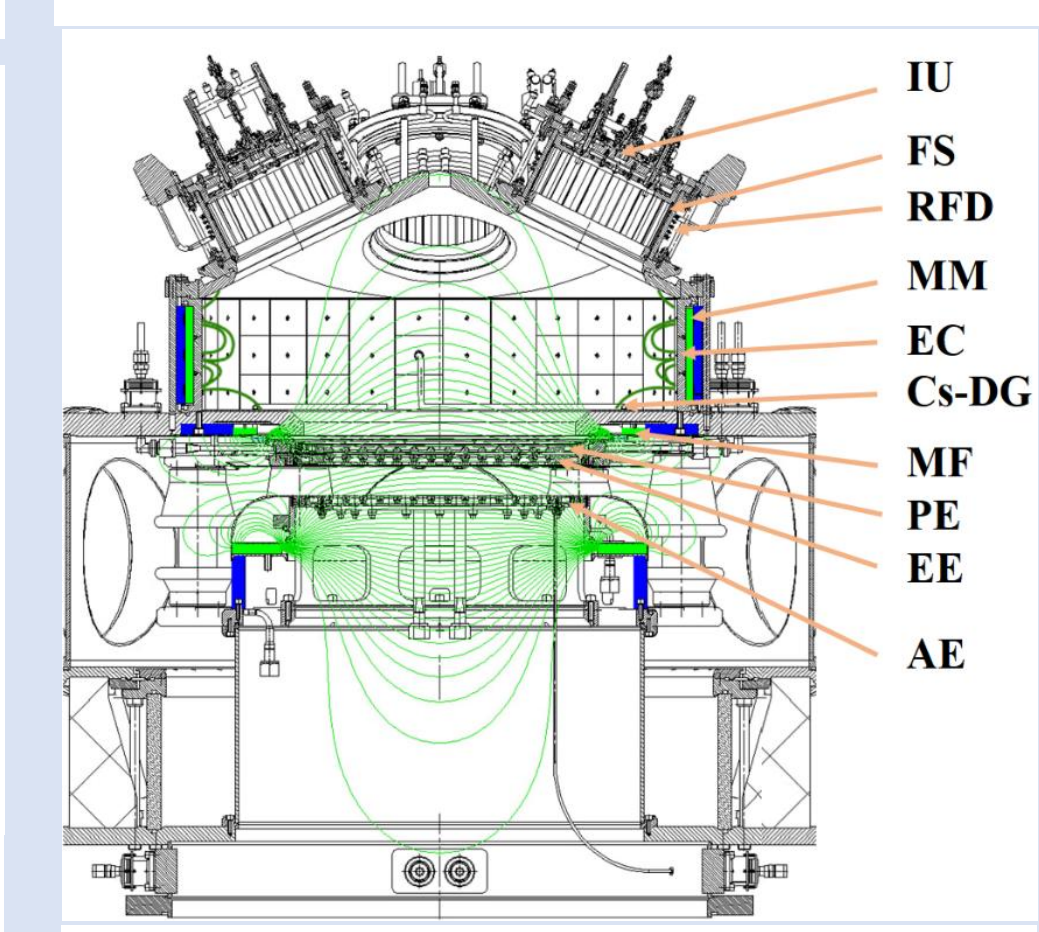
The parameters of the beam formation, efficiencies of the transport and acceleration obtained for various source mosifications are summarized in Table 1. The column I_b shows maximum H- beam current at the source exit, column I_{ag} shows electron current intercepted by acceleration grid, column "Vacuum" corresponds to LEBT tank vacuum. The next three columns show beam transport efficiency to different z-axis positions: to distances 2.5 m, 3.8 m, and 4.45 m. At z = 2.5 m, the current registered by FC is shown. At the other two positions, there are limiting apertures with different sizes indicated in brackets. At z = 4.45 m, the current entering acceleration tube after aperture \emptyset 200 or 260 mm is shown, at 4.45 m – aperture $\emptyset 200 \text{ at accelerator exit.}$

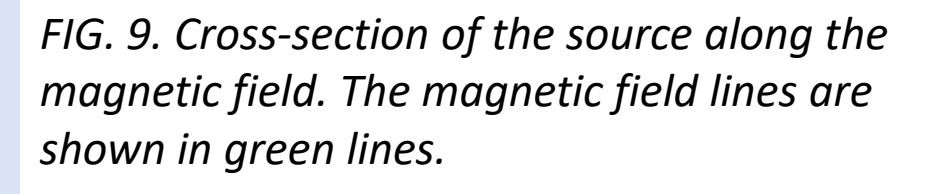
TABLE 1. BEAM PRODUCTION AND TRANSPORT EFFICIENCY

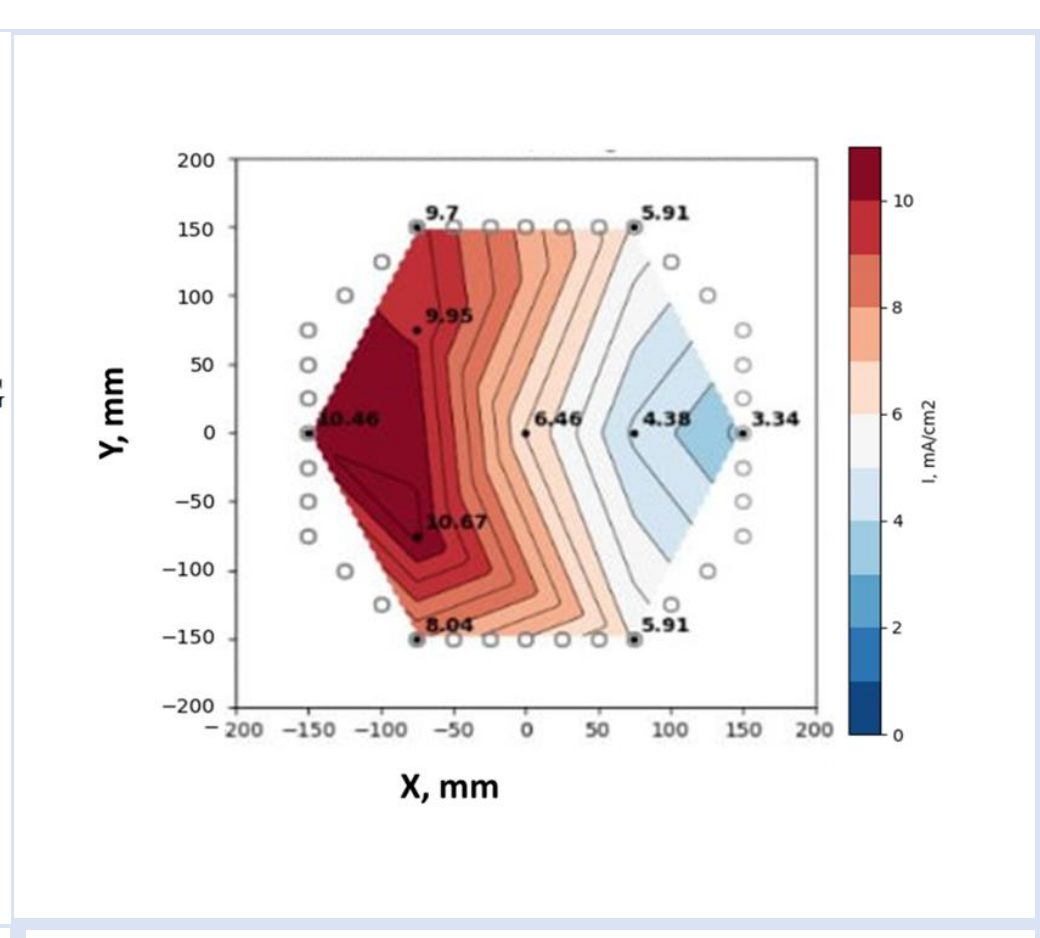
	Acceleration grid	I_b, A $(U_{ex}=14 \text{ kV})$	I _{AG} , A	Vacuum, Pa	$I_{FC}[A]/I_b[A]$ $z = 2.5 \text{ m}$	Accelerator $z=4.5 \text{ m}$	
						$I_p[A]/I_b[A]$	$I_{HV}[A]/I_b[A]$
•	Slits 124 mm	1.5			0.57/1.05	0.6/1.05	0.45/1.05
			0.68	1•10 ⁻³	(ø170)	(ø260)	(ø260)
	Circles ø 16.5 mm	1.5	0.75	1•10-3	0.8/	0.6/1.05	0.6/1.05
					(ø170)	(ø200)	(ø200)
_		1.5	0.75	0.5•10-3		0.79/1.05	0.75/1.05
						(ø260)	(ø260)

9 A NEGATIVE ION SOURCE

The full-scale negative ion source with projected negative ion beam current of 9 A, energy up to 120 keV and pulse duration up to 100 s was designed and manufactured at BINP. The principal scheme if the source is shown in Fig. 9. It includes four RF plasma drivers, an expansion chamber and four-grid IOS with 145 beamlets. Correspondinly the 145 apertures with the internal diameter of 14 mm in the plasma grid are used for beam extraction. Additional pumping is provided at the IOS sides. Thermal stabilization of the IOS grids is provided by circulating a coolant through the internal channels in the grids. A four-channel RF power supply system and HV rectifiers has been manufactured.







grid obtained using a compact plasma grid probes. 4 RF drivers are turned on with total RF power of 120 kW.

FIG. 9. Plasma ion density profile on a plasma

Tests of a full-scale multi-aperture source with a designed beam current of 9 A has been started on a separate stand. Simultaneous operation of four RF plasma drivers was achieved, and the uniformity of plasma flux entering the plasma electrode was studied using grid probes installed in the plasma grid apertures. The probe's small aperture ø4mm allowed local measuring of plasma characteristics. The ion current density distribution near the plasma electrode, measured using 10 probes is shown in Figure 10. The measurements showed 2-3-fold increase in plasma density in the direction of ExB drift. This plasma heterogeneity should have little effect on the uniformity of the beam production, since H- are mainly formed by the conversion of suprathermal hydrogen atoms formed by the dissociation of hydrogen molecules in the RF driver volume.

CONCLUSION

The experiments on negative ion beam production, transport and acceleration have been done at the BINP accelerator test stands. The negative ion beam current of about 1.5 A with emission current density of 450 A/m² was obtained in the prototype source. Efficient suppression of co-extracted electron current at the level of about 1 A was demonstrated. 83% of negative ion source current was transported to the 2.5 m distance from the source, 75% of ion source current - through the acceleration tube entrance. $0.65 \div 0.75$ A beam was accelerated to the energy 0.4 MeV in the pulses with duration 2.5 s. The recorded beam losses are corresponded well to the negative ion stripping on LEBT residual gas.